Structural basis for inhibition of a response regulator of σ^S stability by a ClpXP antiadaptor

Victoria Dorich,[1] Christiane Brugger,[1,3] Arti Tripathi,[2,3] Joel R. Hoskins,[2] Song Tong,[2] Margaret M. Suhanovsky,[1] Amita Sastry,[1] Sue Wickner,[2] Susan Gottesman,[2] and Alexandra M. Deaconescu[1]

[1]Department of Molecular Biology, Cell Biology, and Biochemistry, Brown University, Providence, Rhode Island 02903, USA; [2]Laboratory of Molecular Biology, Center for Cancer Research, National Cancer Institute, Bethesda, Maryland 20892, USA

The stationary phase promoter specificity subunit σ^S (RpoS) is delivered to the ClpXP machinery for degradation dependent on the adaptor RssB. This adaptor-specific degradation of σ^S provides a major point for regulation and transcriptional reprogramming during the general stress response. RssB is an atypical response regulator and the only known ClpXP adaptor that is inhibited by multiple but dissimilar antiadaptors (IraD, IraP, and IraM). These are induced by distinct stress signals and bind to RssB in poorly understood manners to achieve stress-specific inhibition of σ^S turnover. Here we present the first crystal structure of RssB bound to an antiadaptor, the DNA damage-inducible IraD. The structure reveals that RssB adopts a compact closed architecture with extensive interactions between its N-terminal and C-terminal domains. The structural data, together with mechanistic studies, suggest that RssB plasticity, conferred by an interdomain glutamate-rich flexible linker, is critical for regulation of σ^S degradation. Structural modulation of interdomain linkers may thus constitute a general strategy for tuning response regulators.

[*Keywords*: ClpXP; adaptor; antiadaptor; bacteria; biochemistry; crystallography; stress response]

Supplemental material is available for this article.

Received August 27, 2018; revised version accepted March 19, 2019.

In bacteria, the transcriptional reprogramming underlying adaptation to the environment is largely coordinated by σ factors, dissociable promoter specificity subunits that compete with the housekeeping σ^{70} for limited amounts of core RNA polymerase to target it to specific promoters (Maeda et al. 2000; Gruber and Gross 2003). While some σ factors have specific roles in mediating steps in bacterial development, such as in sporulation in *Bacillus subtilis*, or in the response to specific stressors, in *Escherichia coli* and related bacteria, σ^S (also known as RpoS) is the master regulator for the general stress response (Gruber and Gross 2003). σ^S mediates wholesale revamping of the transcriptional program and allows cells to adjust to slowed growth (stationary phase), disappearing critical nutrients, or a variety of stressors, including oxidative damage, pH extremes, and changes in osmolarity (Hengge-Aronis 2002; Battesti et al. 2011). The amount of σ^S is tightly controlled in large part via regulated proteolysis by the ClpXP ATP-dependent protease (Lange and Hengge-Aronis 1991b; Battesti et al. 2011; Mahmoud and Chien 2018). During active growth, σ^S levels are kept low due to its rapid degradation (half-life of ~2 min) by ClpXP. Upon encountering stress or in the stationary phase, σ^S is stabilized to a half-life of >30 min, allowing its levels to rise significantly (Schweder et al. 1996). This regulation is key, as σ^S controls ~10%–23% of the genes in *E. coli* (Lacour and Landini 2004; Patten et al. 2004; Weber et al. 2005; Dong et al. 2008; Dong and Schellhorn 2009; Peano et al. 2015; Wong et al. 2017) and, as a result, is important for many processes, including cross-protection to various environmental stressors, biofilm formation (Adams and McLean 1999) and maturation (Ito et al. 2008), adaptive morphological changes and mutagenesis (Lange and Hengge-Aronis 1991a), the development of antibiotic resistance (Ito et al. 2009), and the persistence and virulence of human enteric and respiratory pathogens as well as animal, insect, and plant pathogens (Dong and Schellhorn 2010).

Efficient σ^S degradation requires the use of a ClpXP adaptor called RssB (Fig. 1A). RssB is a member of the important family of response regulators found in all bacteria.

[3]**These authors contributed equally to this work**
Corresponding author: alexandra_deaconescu@brown.edu
Article published online ahead of print. Article and publication date are online at http://www.genesdev.org/cgi/doi/10.1101/gad.320168.118.

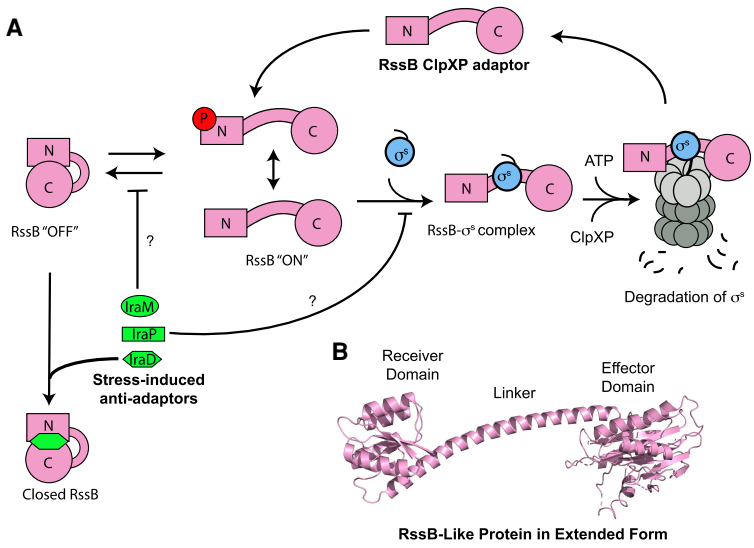

Figure 1. The σ^S degradative pathway in *E. coli*. (*A*) Under active growth, σ^S (blue) is loaded by adaptor RssB (pink) onto ClpXP (gray) for rapid degradation. Exposure to stress signals induces the production of unrelated antiadaptor proteins (IraP, IraM, and IraD; green), which inhibit RssB and block σ^S degradation. RssB phosphorylation (red circle) enhances interactions with σ^S but is not an absolute requirement for regulated turnover (Peterson et al. 2004; Battesti et al. 2013), consistent with a conformational equilibrium model in which RssB can assume the "on" conformation even in the absence of phosphorylation. RssB oligomerization has not been incorporated into this mechanistic scheme, and the role of desphosphoryation in promoting RssB recycling remains unaddressed. "N" and "C" indicate the NTD (receiver domain) and CTD (effector domain) of RssB, respectively. (*B*) Crystal structure of the RssB-like protein from *Pseudomonas aeruginosa* (Protein Data Bank [PDB] ID 3EQ2).

The N-terminal conserved receiver domain of response regulators is generally subject to phosphorylation by sensor histidine kinases (Gao and Stock 2010); the C-terminal effector domain is frequently a DNA-binding domain whose activity is modulated by phosphorylation of the N-terminal domain (NTD) (Galperin 2006; Gao and Stock 2010). In the case of RssB, the C-terminal effector domain (CTD) was predicted to be a degenerate member of the PP2C phosphatase family (Galperin 2006).

RssB is an unusual response regulator and ClpXP adaptor for several reasons: (1) First, as noted above, most response regulators respond to phosphorylation to regulate DNA binding (Galperin 2006). RssB instead mediates protein–protein interactions as the first response regulator to be identified as a ClpXP adaptor (Bearson et al. 1996; Muffler et al. 1996; Pratt and Silhavy 1996; Zhou et al. 2001). In addition, while phosphorylation of RssB occurs, it is not essential for regulation of RssB activity (Peterson et al. 2004; Bougdour et al. 2006). Within the *rssB* operon, no cognate histidine kinase has been identified, although some reports have implicated the ArcB kinase in RssB phosphorylation (Mika and Hengge 2005). (2) RssB has exquisite specificity, with σ^S being the only known substrate that it delivers to ClpXP (Muffler et al. 1996; Pratt and Silhavy 1996; Zhou and Gottesman 1998). (3) Both RssB and σ^S interact weakly with ClpXP, and the weak interactions are stabilized upon ternary RssB•σ^S•ClpX complex formation (Zhou et al. 2001). It has also been proposed that RssB may be a substrate-activating adaptor that induces a conformational change in σ^S to unveil a cryptic ClpXP-binding site in σ^S required for productive loading (Becker et al. 1999; Studemann et al. 2003). (4) Uniquely, unlike other ClpXP adaptors that are regulated via single cognate inhibitors (also known as antiadaptors), RssB is inhibited by multiple unrelated antiadaptors (IraD, IraP, and IraM) that are induced by specific stress signals (Fig. 1A; Battesti and Gottesman 2013; Joshi et al. 2015). These inhibit σ^S degradation in response to SOS-independent DNA damage in the case of IraD (Merrikh et al. 2009), Mg^{2+} starvation in the case of IraM (Bougdour et al. 2008), and phosphate starvation in the case of IraP (Bougdour et al. 2006), allowing intracellular σ^S to rise. Presumably, the generally low levels of RssB, which are under σ^S control, and homeostatic feedback coupling (Pruteanu and Hengge-Aronis 2002) are critical for allowing the antiadaptors to efficiently sequester it.

Processes dependent on response regulators are often tunable and plastic and allow for rapid and reversible adaptation to changing environmental conditions, reflecting both positive and negative regulation by histidine kinases, phosphotransfer domains, phosphatases, or other system-specific regulators (Mitrophanov and Groisman 2008; Battesti et al. 2013). Despite decades of research, the structural basis for this regulation has remained elusive, as only a few structures of response regulator complexes, bound mainly by histidine kinases, have been reported (Casino et al. 2009; Herrou et al. 2012; Trajtenberg et al. 2016). In the context of the general stress response, the lack of structural information on RssB itself, antiadaptors, and RssB•antiadaptor complexes has hampered a mechanistic understanding of how multiple antiadaptors recognize the same RssB target to alter its structure and/or dynamics and achieve stress-specific inhibition. Some structural insights have been provided by two structures of a *Pseudomonas aeruginosa* RssB-like response regulator (Protein Data Bank [PDB] IDs 3EQ2 and 3F7A, deposited by I Levchenko, RA Grant, RT Sauer, and TA Baker, unpubl.) sharing 23% identity with the *E. coli* protein. These structures, derived from two crystal forms (Fig. 1B; Supplemental Fig. S1A,B), show a dimeric and two-domain structure with an extended helical interdomain linker. However, the *P. aeruginosa* protein is not functionally equivalent to RssB (Battesti et al. 2013) and differs from *E. coli* RssB in two important ways: (1) Its active site in the PP2C-like domain is intact. (2) Unlike RssB, its linker features a sequence conducive to parallel coiled-coil formation, stabilized by characteristic "knobs into holes" packing (Supplemental Fig. S1C). Together

with the absence of antiadaptor genes encoded in the *P. aeruginosa* genome, this suggests a different mode of regulation of this homolog and possibly a different function, thus limiting mechanistic comparisons between the two genera.

To shed light on RssB-dependent regulation of σ^S, here we report the crystal structure of the *E. coli* IraD·RssB^{D58P} complex. This reveals a compact RssB architecture featuring extensive interactions between its NTD and CTD, promoted by a closed form of a plastic interdomain linker. Using interdomain disulfide engineering and functional studies, we demonstrate that (1) in the presence of IraD, RssB adopts predominantly a closed conformation; (2) IraD contacts both domains of RssB; and (3) the interactions observed in our structure are crucial for blocking σ^S degradation in vivo and in vitro. Last, we demonstrate that fine-tuning the plasticity of the interdomain glutamate-rich linker plays a critical role in σ^S turnover and, to a lesser extent, its inhibition by antiadaptors. We propose that linker plasticity is conducive to conformational transitions required for substrate handoff and/or recycling and tunes RssB in response to different stress inputs, which, in the case of IraD, involves stabilizing RssB into a closed inactive form. More generally, structural modulation of interdomain linkers may be a widely used strategy for tuning response regulators in bacteria and possibly fungi and plants, which also rely on response regulators for signal transduction.

Results

Structural overview of the IraD·RssB^{D58P} complex

To gain insight into the mechanism of regulation of the RssB adaptor protein by an antiadaptor protein, IraD, we determined the structure of the RssB·IraD complex. We used the nonphosphorylatable RssB^{D58P} variant for cocrystallization with IraD with the expectation of reducing the heterogeneity of the complexes. This expectation was based on previous work that showed that RssB^{D58P} was more susceptible to IraD inhibition than wild type (Battesti et al. 2013) and suggested that IraD may specifically target and stabilize the "off" (nonphosphorylated) conformation of RssB (Fig. 1A). The RssB^{D58P} variant has been shown to be active in vivo and in vitro, although it is somewhat less active than wild type (Battesti et al. 2013). Additionally, we used a truncated proteolytically stable form of IraD: IraD^{Trunc} (residues 17–130). IraD^{Trunc} is competent for binding both RssB and RssB^{D58P}, as determined by pull-down assays and size exclusion chromatography (SEC) (Supplemental Fig. S2A,B). IraD^{Trunc} also inhibits σ^S degradation in vivo and in vitro in a reconstituted degradation assay using purified proteins (Supplemental Fig. S2C–F). Using cells coexpressing RssB^{D58P} and IraD^{Trunc}, we isolated an in vivo assembled complex of RssB and IraD^{Trunc}. We determined the structure of this complex using single-wavelength anomalous diffraction at the K edge of selenium at a resolution of 2.6 Å followed by refinement against a higher-resolution (2.0 Å) data set (Table 1). The crystal asymmetric unit featured one compact trefoil-shaped heterodimer (Fig. 2B), consistent with our SEC data (Supplemental Fig. S2B) and a previous report that indicated a 1:1 stoichiometry of IraD to RssB (Micevski et al. 2015).

Two lobes of the trefoil belong to RssB and are formed by its two domains: the α/β NTD (RssB NTD), which resembles other receiver domains and contains the phosphotransfer site at the end of strand β3, and the CTD (RssB CTD), which is formed by two β sheets of mixed polarity buttressed on one side by α helices α8 and α9 (Fig. 2B–D). The complex is organized around a core of helices (Fig. 2C,D) that pack against each other through dry interfaces. The receiver domain from full-length RssB^{D58P} overlays well (RMSD of 0.6 Å) over the previously determined structure of the isolated wild-type NTD containing the phosphoacceptor aspartate (PDB ID 3EOD, deposited by I Levchenko, RA Grant, RT Sauer, and TA Baker, unpubl.). However, in our structure, the β3–α3 and β5–α5 loops are well ordered, while in the isolated NTD, they remained unmodeled (Supplemental Fig. S3A,B). Subtle differences affecting the phosphorylation site residues exist, but, due to sequence divergence in switch regions between RssB and well-understood response regulators such as CheY, we exercise caution in interpreting them.

Despite low sequence identity (<10%), the RssB CTD shares strong structural similarity to PPM phosphatases, such as bacterial sporulation phosphatase SpoIIE, consistent with previous predictions (Galperin 2006). The RssB CTD similarity to phosphatase domains extends beyond general architecture and has relevance for RssB regulation. Like the RssB CTD, SpoIIE contains two switch helices embedded within the phosphatase fold, which connects to a regulatory domain via a long α helix (Supplemental Fig. S3C). The switch helices undergo rotation during SpoIIE activation to promote dimerization (Supplemental Fig. S3C,D), donate functional groups, and complete the Mn^{2+} coordination sphere required for catalysis (Bradshaw et al. 2017). Unlike SpoIIE, *E. coli* RssB is a pseudophosphatase, as it lacks some of the catalytic aspartates critical for Mn^{2+} binding. However, an intriguing feature of both proteins is the formation of a hydrophobic network of residues in the interdomain linker and switch helices (Supplemental Fig. S3E). In SpoIIE, these form part of the dimerization interface and are key to function (Bradshaw et al. 2017). Equivalent residues (V120, L124, M128, L139, L222, and L226) (Supplemental Fig. S3F) are not stringently conserved between RssB and SpoIIE but largely maintain their hydrophobicity to establish an extensive long-range network of hydrophobic contacts that link switch helix α8 in the RssB CTD to helix α5 in the RssB NTD. It is striking that a cluster of substitutions in this region (L214H, A216T, L218V, A221T, and Q254K) leads to resistance to IraD regulation but not compromised IraD binding in vivo or in vitro (Battesti et al. 2013). They likely cause a shift in the conformational equilibrium of RssB toward the activated "on" form with high affinity for σ^S, similar to what is normally brought about by phosphorylation (Fig. 1A).

The third lobe of the trefoil is formed by IraD, which contacts both RssB lobes via a well-ordered recognition

Table 1. *Crystallographic data and refinement statistics*

	$IraD^{Trunc}$·$RssB^{D58P}$ data set 1	$IraD^{Trunc}$·$RssB^{D58P}$ data set 2
Data collection		
Space group	$P4_32_12$	$P4_32_12$
Cell dimensions		
a,b,c[a]	55.7 Å, 55.7 Å, 299.8 Å	55.9 Å, 55.9 Å, 300.3 Å
α,β,γ	90.0°, 90.0°, 90.0°	90.0°, 90.0°, 90.0°
Wavelength	0.97918 Å	1 Å
Resolution	39.4 Å–2.6 Å	29.1 Å–2.0 Å
R_{sym}[b]	0.111 (0.885)	0.076 (0.689)
$\langle I/\sigma_I \rangle$	21.8 (2.82)	25.0 (1.95)
Completeness	97.6% (80%)	96.9% (92.9%)
Redundancy	20.4 (11.8)	7.4 (5.6)
Phasing FOM	0.31	
Number of reflections/unique reflections	22,525,594/24,488	240,260/32,605
Refinement		
Resolution		29.1 Å–2.0 Å
Number of reflections used		32,605 (3053)
R_{work}/R_{free}[c]		20.00%/24.50%
Number of atoms		
Protein		3355
Water		125
B factors		
Protein		58.7 $Å^2$
Water		51.6 $Å^2$
RMSD		
Bond lengths		0.008 Å
Bond angles		0.938°
Coordinate error[d]		0.19 Å
Ramachandran plot analysis		
Preferred		97.5%
Allowed		2.3%
Disallowed		0.0%
Rotamer outliers		0.0%
MolProbity clash score		5.01

[a]Values in parenthesis are for highest-resolution shell.
[b]$R_{sym} = (\Sigma|I - \langle I \rangle|/\Sigma\langle I \rangle)$, where I refers to the observed intensity, and $\langle I \rangle$ refers to the average intensity of multiple measurements of the same reflection.
[c]$R_{free} = (\Sigma|F_o - F_c|/\Sigma|F_o|)$. R_{free} was calculated by omitting 5.5% of the data from refinement.
[d]Maximum likelihood.

helix (a3). Additional contacts with the RssB NTD are via IraD a2 (Fig. 2B). Overall, the $IraD^{Trunc}$·$RssB^{D58P}$ complex buries a total surface area of ~2100 $Å^2$, consistent with its stability in solution (Janin et al. 1988). The IraD fold (an antiparallel β sheet flanked by three α helices) resembles the T4 phage protein Gp25 homodimer, with which it shares 15% identity. Gp25 homologs are required for sheath polymerization and attachment of the sheath to the phage baseplate (Basler et al. 2012). Gp25 is structurally related to baseplate components of type VI secretion systems, such as *P. aeruginosa* HsiF, but details of the interactions of Gp25-like proteins with binding partners have not been defined at atomic resolution. Interestingly, both Gp25 and IraD contain a strictly conserved EPRI motif also found in HsiF (Supplemental Fig. S3G). In HsiF, the conserved glutamate of the EPRI motif is important for type VI secretion in vivo (Lossi et al. 2011), but the precise mechanism behind the functional defect of the variant with a glutamate substitution remains unknown. In crystallized Gp25, the EPRI motif together with a1, the a1–a2 loop, and a3 is part of the dimerization interface (Supplemental Fig. S3H). In IraD, the EPRI motif forms a loop connecting helix a3 to strand b1 (Fig. 2B), both of which make contact with RssB. We note that the region of highest divergence between IraD and Gp25 is the N terminus, which features a long tail in IraD susceptible to proteolysis in vivo; this was deleted in our $IraD^{Trunc}$ construct. This region likely samples multiple conformations. Although not directly at the interface with RssB, this tail appears to modulate RssB inhibition, since $IraD^{Trunc}$ is a more potent inhibitor of RssB than IraD in vitro (Supplemental Fig. S2F).

When bound to IraD, RssB assumes a closed conformation

An unanticipated feature of the $IraD^{Trunc}$·$RssB^{D58P}$ complex is the compact conformation of $RssB^{D58P}$ (Fig. 2B–

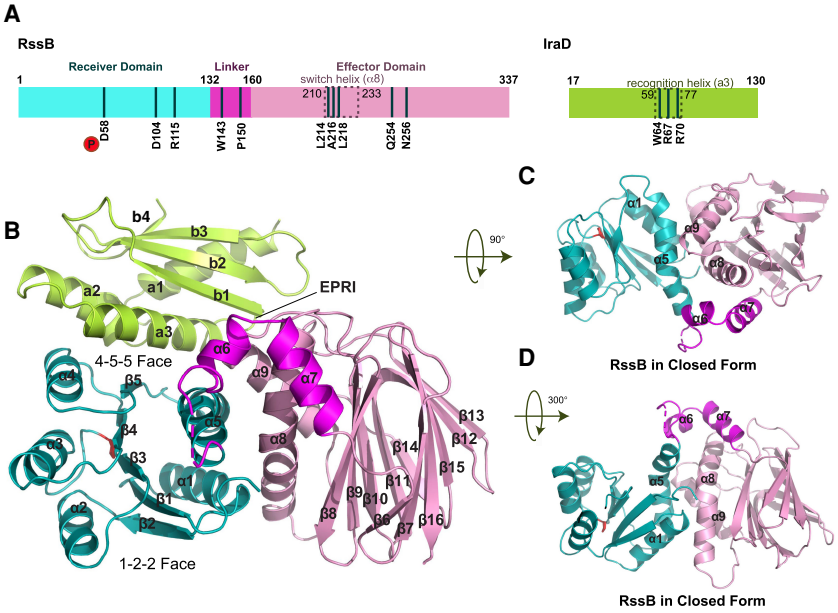

Figure 2. Overall architecture of the IraD^{Trunc}·RssB^{D58P} complex. (*A*) Schematics of *E. coli* RssB and IraD domain architecture. Indicated are the phosphoacceptor residue D58 and mutations in the RssB switch helix (α8) that lead to resistance to IraD in vivo and/or in vitro (Battesti et al. 2013) characterized in this study. Also shown is IraD, including the IraD recognition helix (a3) and residues mutated here. Dotted lines indicate the boundaries of the RssB switch and IraD recognition helices. (*B*) Front view of *E. coli* IraD (residues 18–124; green) bound to the RssB^{D58P} variant (residues 3–337; color-coded as in *A*). Disordered residues that could not be built reliably into electrondensity are indicated by a dashed curve. P58 (D58 in wild-type RssB) is shown in red stick representation. (*C*,*D*) Side view of RssB. The IraD chain has been removed to allow a view of the core of RssB, composed of α1, α5, α8, and α9.

D). Despite significant efforts, free *E. coli* RssB has long resisted structural analyses; therefore, we compared our structure with that of the previously crystallized *P. aeruginosa* homolog. In our structure, the linker folds into two short helices (α6–α7) (Fig. 2B) that, together with α5, juxtapose the RssB NTD to the CTD. Residues 135–137 preceding α6 were disordered and could not be modeled.

To establish whether the closed conformation seen for crystallized RssB^{D58P} is also populated in solution and in the absence of IraD, we probed conformational dynamics in solution using interdomain disulfide cross-linking. We engineered an RssB variant, RssB^{CC} carrying the S29C and E229C substitutions and the native D58 residue rather than the D58P substitution used for crystallization (Fig. 3A). RssB^{CC} is active, as assessed by its ability to participate in σ^S degradation in vivo, bind IraD in vivo (Supplemental Fig. S4A,B), and act with ClpXP to degrade σ^S in vitro (Supplemental Fig. S4C; Supplemental Table S1). We had the following expectation: When bound to IraD, RssB^{CC} will assume a closed conformation that will cross-link the RssB NTD and CTD in the presence of atmospheric oxygen and a catalyst, such as copper (1,10)-phenanthroline (CuPhen). The open conformation observed in the *P. aeruginosa* homolog is incompatible with formation of the engineered intramolecular disulfide, while the intercysteine distance in IraD·RssB^{CC} is predicted, on geometry considerations, to be conducive to disulfide formation (Fig. 3A,B). In the presence of CuPhen and IraD·RssB^{CC}, we observed clear formation of a faster-migrating electrophoretic species (Fig. 3C, lane 7). This was not apparent with either wild-type or single-variant complexes (Fig. 3D–F, lane 7). When we compared cross-linking of IraD-bound and free RssB^{CC}, we noticed less intramolecular cross-linking in free RssB^{CC} (~55% vs. 18%) (Fig. 3G, lanes 8,9).

Together with LC-MS/MS analysis of in-gel trypsin/AspN-treated IraD·RssB^{CC} (Supplemental Fig. S4D), these data indicate that the engineered disulfide is not only intramolecular but also specific. We also observed intermolecular RssB cross-linking with free RssB and RssB^{CC}, resulting in detection of a minor species consistent with the molecular weight of a dimer (Fig. 3G, lanes 9,10). Thus, we conclude that in the presence of IraD, the closed conformation seen in crystallo also occurs in solution and that the D58P mutation is not required for this. These data also indicate that free RssB exists in a conformational equilibrium of open and closed forms that are predominantly monomeric but can also self-associate into scarce transient dimers.

IraD W64 is key for complex formation

We next sought to define IraD residues critical for RssB recognition. IraD straddles both domains of RssB and interacts primarily through a2 and the recognition a3 helix (Figs. 2B, 4A). The recognition helix is wedged in a groove in between the RssB NTD and CTD and makes contact with the base of the linker helix α5 and β5. The binding interface largely overlaps with the α4–β5–α5 face of RssB (referred to here as the 4-5-5 face in agreement with response regulator nomenclature), which in many response regulators supports dimerization and/or association with binding partners (Gao and Stock 2010). The area buried by IraD binding to the RssB NTD is significantly larger than that buried by the RssB CTD (~1330 Å^2 vs. ~830 Å^2), consistent with two-hybrid analyses and pull-down assays that showed that IraD interacts with the isolated NTD but not the isolated CTD (Battesti et al. 2013; Micevski et al. 2015). Interactions between the RssB NTD and IraD are provided by invariant R115 and D104, which are involved in hydrogen bonds and cation–π interactions with IraD F75 and in hydrogen bonds and salt bridges with IraD R67, Q68, and W64. CTD interactions are

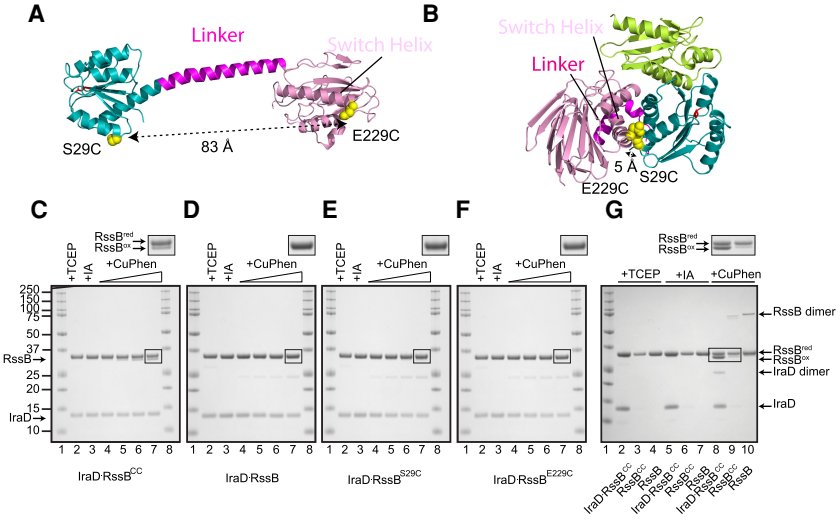

Figure 3. IraD stabilizes a closed and novel RssB conformation. (*A*) Model of open RssB obtained using Phyre[2] (Kelley et al. 2015) based on the *P. aeruginosa* protein model (PDB ID 3EQ2) showing the location of the two cysteine substitutions S29C and E229C in yellow CPK models, which are predicted to be too far apart to cross-link. Domains are colored as in Figure 2A. (*B*) View of the closed IraD-bound RssB conformation highlighting a Cα–Cα distance compatible with a disulfide (Cα–Cα distances range from 5.2 to 6.1 Å) (Trivedi et al. 2009). Domains area colored as in Figure 2A, and residues substituted for cysteine are shown as yellow CPK models. (*C–F*). Nonreducing SDS-PAGE of CuPhen-catalyzed oxidation reactions with the in vivo assembled purified IraD^{Trunc}·RssB^{CC} complex (*C*) and wild-type (*D*) or single Cys variant RssB (RssB^{S29C} [*E*] or RssB^{E229C} [*F*]) complexes. Purified protein was first reduced with TCEP, then subjected to oxidation at CuPhen concentrations ranging from 0 to 20 µM for 20 min at room temperature, and blocked with iodoacetamide (IA). A doublet is present only in oxidized IraD^{Trunc}·RssB^{CC}. Boxed bands are shown at higher magnification as *insets* in the *top right* corners of the gels. (*G*) Nonreducing SDS-PAGE of oxidation reactions with purified free and IraD-bound wild type and RssB^{CC} and 15 µM CuPhen. Boxed RssB bands are shown at higher magnification in the *top right* corner.

conferred primarily by Q254 and N256, which bond to IraD R70, S71, and Q84 (Fig. 4A).

Previous studies had demonstrated interactions of IraD with the RssB NTD but not with the RssB CTD (Battesti et al. 2013; Micevski et al. 2015). Our structure, however, suggests important contacts of the recognition helix with both the NTD and the CTD. Using pull-down assays carried out with purified RssB and His-tagged IraD variants, we established that IraD W64, R67, and R70 are critical for the interaction and that the W64R substitution variant is the most defective in interaction (Fig. 4B; Supplemental Fig. S5A). The functional impairment observed here is likely not due to improper folding, as demonstrated using circular dichroism (Supplemental Fig. S5B). We then assessed the function of selected IraD variants in vivo and in vitro. The in vivo assay (see the Materials and Methods) relied on quantifying σ^S degradation over time following inhibition of protein synthesis via Western blot analysis of induced cells transformed with an IPTG-inducible high-copy plasmid encoding for wild-type or variant IraD carrying substitutions in the critical IraD residues. We carried out these studies in two different strains: AB007 (*rssB*$^+$) expressing native levels of RssB and AB011 (*rssB*^{UP}) containing constitutively higher levels of RssB (Bougdour et al. 2006). In both strains, the W64R substitution led to a pronounced functional defect, resulting in little σ^S stabilization (Fig. 4C,D; Supplemental Fig. S5C). We note that these data were obtained under conditions of IraD overproduction, which is likely to suppress partial defects. The other substitutions caused more subtle defects, which were apparent only in the *rssB*^{UP} strain at higher levels of RssB. These results are consistent with the multiple interactions of W64 with RssB I94, V105, and D104 observed in our X-ray structure as well as our pull-down assay (Fig. 4B; Supplemental Fig. S5A).

To probe IraD function in vitro, we monitored IraD's ability to inhibit degradation of σ^S in the presence of ClpXP, RssB, ATP, and acetyl phosphate (Fig. 4E), which supports RssB phosphorylation (Bouché et al. 1998). At concentrations of IraD that completely inhibit σ^S degradation, we observed that IraD^{W64R} inhibited degradation ~20% (Fig. 4E), consistent with the severe binding defect of this variant in vitro (Fig. 4B) and its lack of function in vivo (Fig. 4C,D). There was also partial inhibition by IraD^{R67A} and IraD^{R70A} both in vivo (Fig. 4C,D) and in vitro (Fig. 4E). Thus, we conclude that R67 and R70 and particularly W64 are important for RssB recognition.

RssB-D104 is key for RssB:antiadaptor complex formation

To dissect binding determinants on RssB, we targeted for mutagenesis residues seen at the IraD–RssB interface within both the RssB NTD (D104 and R115) and the RssB CTD (Q254 and N256), as shown in Figure 4A, and carried out tests of these mutant proteins in vitro and in vivo (Fig. 5). From initial pull-down experiments with lysates coexpressing His-tagged IraD and either wild-type or variant RssB, D104 was identified as critical for the interaction with IraD. Slightly decreased interactions were observed with RssB^{Q254A}, RssB^{N256A}, and the RssB$^{Q254A\ N256A}$ variant, and no significant decrease was seen with RssB^{R115A} (Supplemental Fig. S6A,B). Further tests focused on RssB^{D104N}, RssB^{R115A}, and the double CTD mutant RssB$^{Q254A\ N256A}$. These proteins were purified and shown to have CD spectra similar to wild type (Supplemental Fig. S6C). Their interaction with IraD was tested. RssB^{D104N} showed reduced binding to IraD, RssB$^{Q254A\ N256A}$ had modestly reduced interaction, and RssB^{R115A} had no

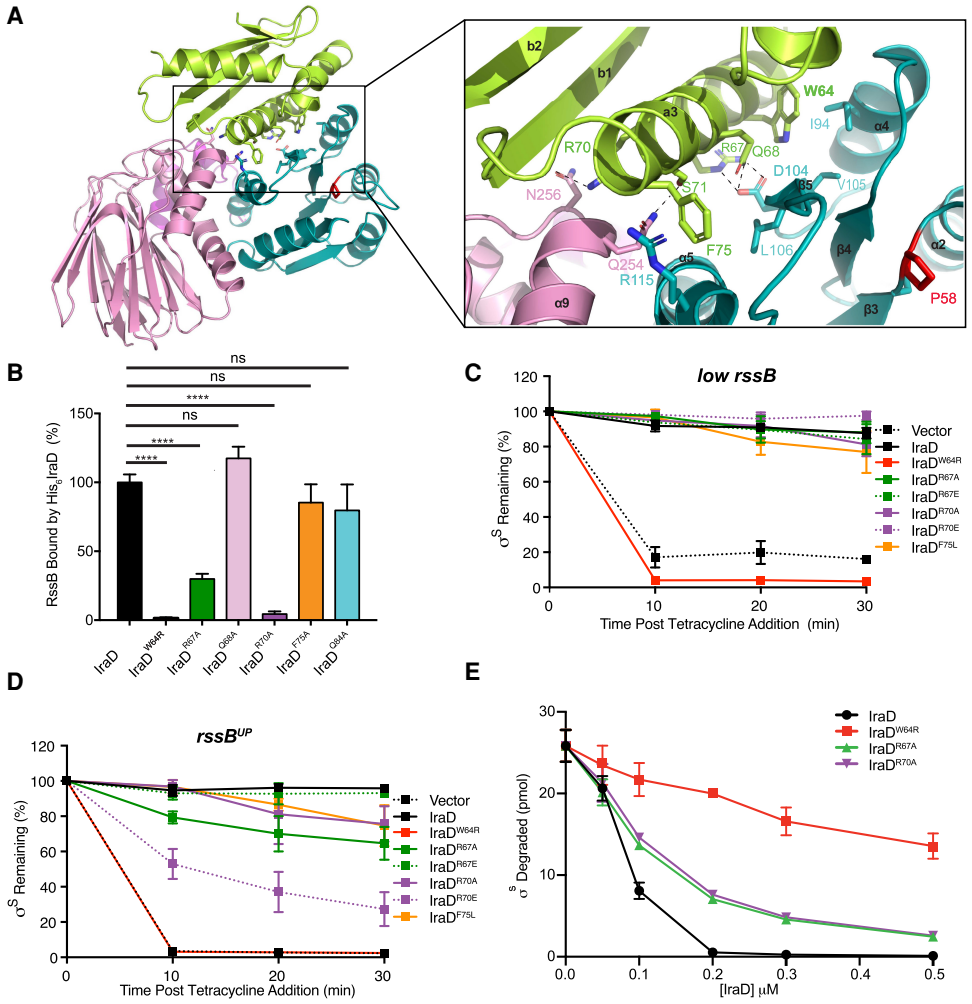

Figure 4. IraD residues W64, R67, and R70 serve as a recognition triad. (*A*) IraD^{Trunc}·RssB^{D58P}, colored as in Figure 2B, with a close-up view of the IraD^{Trunc}–RssB^{D58P} interface. Residues targeted for mutagenesis and P58 are shown as sticks. P58 is colored red. (*B*) Quantification of pull-down assays of wild-type RssB with purified His$_6$IraD mutants. RssB binding was normalized to the amount of wild-type RssB bound to wild-type His$_6$-tagged IraD. A sample SDS-PAGE gel is shown in Supplemental Figure S5A. Statistical significance (*P*-value < 0.05) was established using a one-way ANOVA test. Shown are means with SD. $n = 3$. (****) $P < 0.0001$. (*C*,*D*) Quantification of σ^S turnover in strain AB007 (low *rssB*) expressing inducible wild-type and mutant IraD alleles and physiological levels of RssB (*C*) and strain AB011 (*rssB^{UP}*) overexpressing RssB (*D*). IraD was expressed from induced pQE-IraD, and mutant derivatives were expressed from pST5001–pST5006. Cells were treated with tetracycline, and the remaining σ^S during the chase was determined as described in the Materials and Methods. Shown are means with SD. $n = 3$. (*E*) Inhibition of RssB-dependent σ^s degradation by wild-type or variant IraD in vitro. σ^S degradation by ClpXP was performed as described in the Materials and Methods in the presence of 0.1 μM ClpX, 0.2 μM ClpP, 2.4 μM Alexa488-σ^S, 0.1 μM RssB, and IraD wild type or variant, as indicated. Data from three replicates are presented as mean ± SD. Some error bars are obscured by plot symbols.

detectable decrease in interaction (Fig. 5A; Supplemental Fig. S6D).

Each of these RssB alleles was tested in vivo for activity and sensitivity to each of the antiadaptors. RssB mutants and the wild-type control were expressed on plasmid pHDB3 from the native *rssB* promoter, and the degradation of σ^S was determined after treatment of cells with chloramphenicol to block further protein synthesis. In addition to the alleles discussed above, RssB^{L218V}, a previously studied RssB mutant found to be resistant to all three antiadaptors (Battesti et al. 2013), was included as a positive control. In the strain used in Figure 5B, not exposed to any stress, none of the antiadaptors should be significantly induced (Bougdour et al. 2008). All tested alleles except D104A were active for σ^S degradation in this strain (Fig. 5B; Supplemental Fig. S6E). To test for sensitivity to IraD in vivo, we also monitored activity in strain AT477 (*iraD^{UP}*), in which *iraD* was placed under the control of a tunable arabinose-responsive pBAD promoter. Under these conditions, the degradation of σ^S was inhibited when wild-type RssB was expressed, but RssB^{L218V} was resistant, as observed previously (Fig. 5C; Supplemental Fig. S7A; Battesti et al. 2013). We observed pronounced resistance to IraD for RssB^{D104N}, RssB^{R115A}, and RssB$^{Q254A\ N256A}$, fully

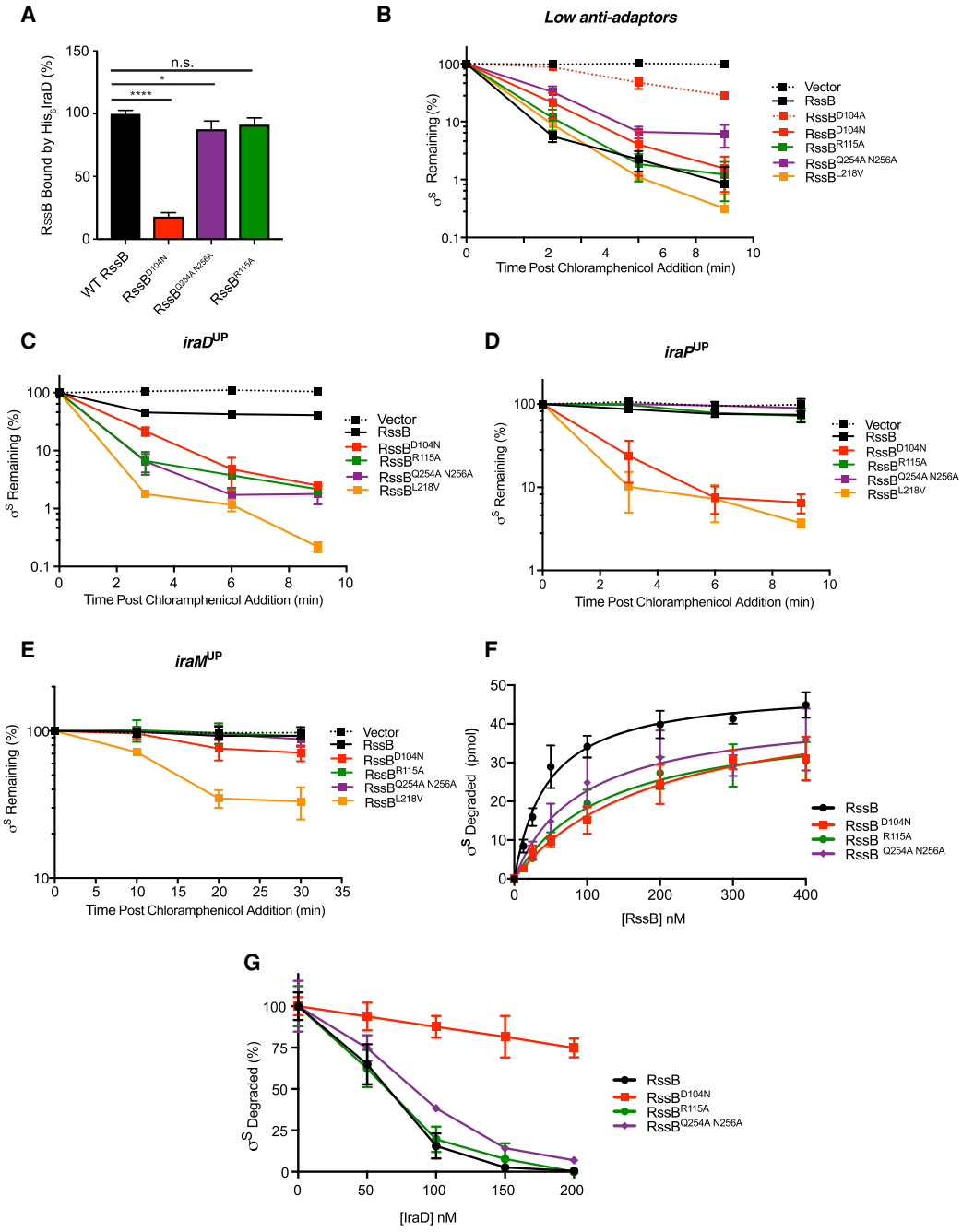

Figure 5. RssB-D104 is key for antiadaptor interactions. (*A*) Quantification of pull-down assays using purified His-tagged IraD and wild-type or variant RssB. $n = 3$. Sample SDS-PAGE analyses are shown in Supplemental Figure S6D. Statistical significance was calculated using a one-way ANOVA test. (****) *P*-value <0.0001; (*) *P*-value <0.05; (n.s.) *P*-value >0.05. (*B–E*). Degradation of σ^S in cells expressing wild-type or variant RssB in a strain expressing only low levels of antiadaptors (*B*) or in the presence of specific antiadaptors (*C–E*). *rssB* alleles were overexpressed from pHDB3 plasmids (pW6, RssB; pST4002, $RssB^{D104A}$; pST4003, $RssB^{D104N}$; pST4004, $RssBD^{115A}$; pST4007, $RssB^{Q254A\ N256A}$; and pBA465, $RssB^{L218V}$) (see Supplemental Table S3) in which RssB is expressed from its native promoter in low anti-adaptor strain ST1005 (*B*), $iraD^{UP}$ strain AT477 (*C*), $iraP^{UP}$ strain ST1011 (*D*), and $iraM^{UP}$ strain BA290 (*E*) (Supplemental Table S4). (*F*) In vitro degradation of σ^S by ClpXP and RssB, $RssB^{D104N}$, $RssB^{Q254A\ N256A}$, or $RssB^{R115A}$. End point assays within the linear phase of degradation were performed as described in the Materials and Methods in the presence of 0.1 µM ClpX, 0.2 µM ClpP, 2.4 µM Alexa488-σ^S, and wild-type RssB or RssB variant as indicated. Data from three replicates are presented as mean ± SD and were fit to the Michaelis-Menten equation using Prism. V_{max} and K_M values are shown in Supplemental Table S1. (*G*) In vitro IraD inhibition of RssB-dependent σ^S degradation by ClpXP in the presence of RssB, $RssB^{D104N}$, $RssB^{Q254A\ N256A}$, or $RssB^{R115A}$. Degradation was performed as described for *F* using 0.1 µM wild-type RssB or RssB mutant and IraD as indicated. For each RssB protein, degradation in the absence of IraD was set to 100%; 36 pmol (±3 pmol) for RssB, 28 pmol (±1 pmol) for $RssB^{D104N}$, 27 pmol (±4 pmol) for $RssB^{Q254A\ N256A}$, and 28 pmol (±3 pmol) for $RssB^{R115A}$. Data from three or more replicates are presented as mean ± SD. Some error bars are obscured by plot symbols.

consistent with predictions from the cocrystal. We extended our in vivo analysis of antiadaptor sensitivity to IraP and IraM and determined that D104 also plays a key role in sensitivity to IraP but not IraM (Fig. 5D,E).

Purified RssB^{D104N}, RssB^{R115A}, and RssB$^{Q254A\ N256A}$ were also assessed for their function in σ^S degradation in vitro (Fig. 5F). As was the case in vivo, these mutants all remain competent for degradation of σ^S by ClpXP, although they showed slightly decreased activity compared with wild type (Fig. 5F; Supplemental Table S1). As expected, RssB^{D104N} was resistant to IraD regulation (Fig. 5G). Consistent with the effect on IraD function, D104 in the RssB NTD makes multiple interactions with IraD, including van der Waals contacts with W64 and hydrogen bonds with Q68 and R67 (Fig. 4A), and is highly compromised in pull-down assays done with purified proteins (18% ± 3% binding relative to wild type) (Fig. 5A). Like wild type, RssB^{D104N} retains the ability to be stimulated by acetyl phosphate in vitro (Supplemental Fig. S8A), suggesting that, at some level, interdomain communication and conformational switching between an "off" and "on" state are still possible in this variant. However, RssB^{D104N} is more resistant to trypsin than wild type (Supplemental Fig. S8B,C). While the disruptive effect of D104 mutants on antiadaptor action may thus be principally explained by a direct disruption of the binding interface in the case of IraD, in the case of IraP, indirect conformational mechanisms may also be at play. Consistent with important roles for this region of RssB, the RssB NTD carrying a substitution of a neighboring residue (L106D) (Fig. 4A) on the 4-5-5 RssB face was shown previously to be deficient for interaction with IraD, while a variant carrying a substitution on the opposite side (L36D) on the 1-2-2 face (Fig. 2B) was still able to interact (Micevski et al. 2015). RssB$^{Q254A\ N256A}$ was modestly resistant to IraD (Fig. 5G), consistent with resistance in vivo (Fig. 5C) and a decrease in interaction (Fig. 5A); RssB^{R115A} was not detectably resistant in vitro.

Thus, our data altogether indicate that IraD contacts with the RssB NTD revealed by our structure are critical for function and that regulation by IraD is also modulated by interaction with the RssB CTD.

The glutamate-rich interdomain linker is key for activity and modulates RssB inhibition

One interpretation of our results suggests that long-range interdomain communication and large conformational transitions in the RssB linker are important for antiadaptor function. Consistent with this, a W143R mutation at the N-terminal end of α6 in RssB (Figs. 2B, 6A) compromises IraD regulation (Battesti et al. 2013). In addition, RssB^{P150T} carrying a substitution mapping to the loop connecting α6 to α7 (Fig. 6A) is also resistant to IraD regulation (Battesti et al. 2013). Notably, the α5–α6 loop also contains a low-complexity E134–E137 polyglutamate motif (Supplemental Fig. S1C). Polyglutamate stretches are known to serve as plastic linkages with potential for helix-to-coil transitions due to destabilization of helicity through side chain electrostatic repulsion (Daggett et al. 1991; Krejtschi and Hauser 2011). Consistent with this plasticity, the electron density in this region was of poor quality and could not be modeled reliably. We reasoned that by substituting the linker glutamates with residues with good propensity for α-helix formation, we might be able to stabilize helicity and favor a more open and rigid RssB conformation. We chose a triple alanine substitution, due not in small part to the fact that RssB also possess a low-complexity well-ordered AAAA motif (residues A151–A154) that is located at the N terminus of α7 and is entirely α-helical (Fig. 6A). We chose to mutate three of the four glutamates in the E134–E137 stretch, generating an EAAA motif that has been established to fold as a rigid helical linker in multiple contexts (Chen et al. 2013). This construct is referred to as RssB^{AAA}. In parallel, we also created a RssB^{GSGS} variant in which residues E134–E137 were replaced by a flexible GSGS sequence (Chen et al. 2013). While RssB^{AAA} can promote σ^S degradation by ClpXP in an in vitro degradation assay, it exhibits significantly less activity than wild type both in vivo and in vitro (Fig. 6B,C; Supplemental Table S1). However, it binds σ^S as well as wild type in a bacterial two-hybrid assay (Supplemental Fig. S9A). This region may thus provide functionally critical sequence-specific interactions and/or confer the necessary plasticity for productive loading and handoff of σ^S to ClpXP.

The GSGS linker mutant RssB^{GSGS} also affects RssB function (Fig. 6B). RssB^{GSGS} has reduced ability to bind σ^S in a bacterial two-hybrid assay (Supplemental Fig. S9A) and is incapable of promoting degradation of σ^S in vivo (data not shown) or in vitro (Fig. 6B), highlighting the importance of the residues in the linker. RssB^{GSGS} is much more susceptible to trypsin proteolysis than wild type (Supplemental Fig. S9B), consistent with decoupling of the RssB NTD from the CTD and a more solvent-accessible flexible linker. We observed no evidence of altered oligomerization relative to wild-type RssB in either of these constructs by gel filtration or chemical cross-linking, and wild-type RssB was determined to be monomeric by SEC-MALS (SEC with multiangle light scattering) (Supplemental Fig. S10). Thus, protection of wild-type RssB does not stem from oligomerization but rather distinct intramolecular rearrangements. In vivo, the reduced activity of RssB^{AAA} makes sensitivity to antiadaptors more difficult to assess, but it appears to be sensitive to regulation by all antiadaptors (Fig. 6C,D; Supplemental Fig. S11). In vitro, RssB^{AAA} is modestly more resistant to IraD inhibition than wild type (Fig. 6E). Finally, while overall expression of RssB^{AAA} is lower than for wild-type RssB, complicating the assessment of IraD binding in lysates (Supplemental Fig. S9C), pull-down assays with purified protein demonstrate a modest defect in binding IraD (Fig. 6F; Supplemental Fig. S9D).

Discussion

General stress responses in all bacteria are pivotal for adaptation to the environment as well as for mediating host–microbe interactions and often connect signaling by

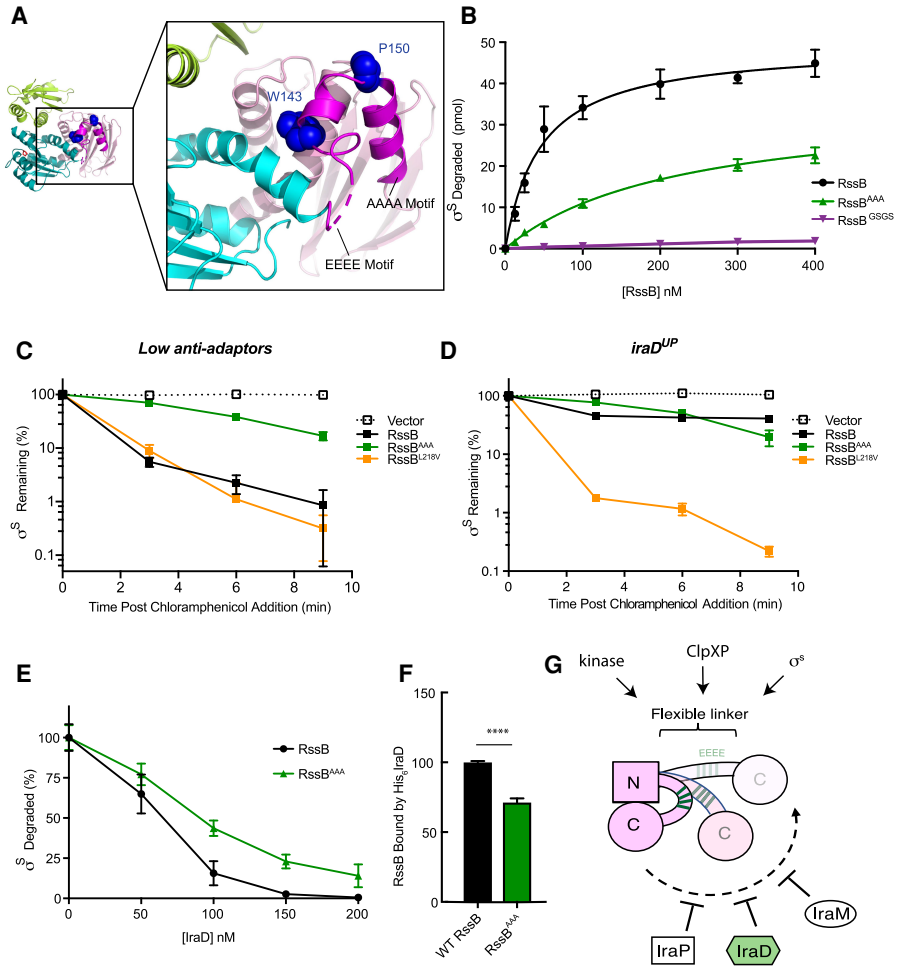

Figure 6. The interdomain linker is key for σ^S turnover. (*A*) The IraD^{Trunc}·RssB^{D58P} structure and a close-up view of the interdomain helical linker (magenta), with residues implicated previously in antiadaptor regulation (Battesti et al. 2013) shown as blue CPK models. Disordered residues, including the polyglutamate motif, are shown as a dashed line. IraD and RssB domains are colored as in Figure 2B. (*B*) In vitro degradation of σ^S by ClpXP and RssB, RssB^{AAA}, or RssB^{GSGS}. End point assays within the linear phase of degradation were performed as described in the Materials and Methods in the presence of 0.1 µM ClpX, 0.2 µM ClpP, 2.4 µM Alexa488-σ^S, and wild-type or variant RssB as indicated. Data from three replicates are presented as mean ± SD and were fit to the Michaelis-Menten equation using Prism. V_{max} and K_M values are shown in Supplemental Table S1. Some error bars are obscured by plot symbols. (*C,D*) Quantification of σ^S degradation in vivo in the presence of wild-type or variant RssB. Plasmid-borne *rssB* alleles were overexpressed using pHDB3 plasmids (pW6, RssB$^+$; pAT329, RssB^{AAA}; and pBA465, RssB^{L218V}) (see Supplemental Table S3) in low antiadaptor strain ST1005 and *iraD^{UP}* strain AT477 as described in the Materials and Methods. (*E*) In vitro IraD inhibition of σ^S degradation by ClpXP in the presence of wild-type RssB or RssB^{AAA}. Degradation was performed as described for *B* using 0.1 µM RssB or RssB^{AAA} and IraD as indicated. Degradation in the absence of IraD was set to 100%; 36 pmol (±3 pmol) for RssB and 18 pmol (±1 pmol) for RssB^{AAA}. Data from three or more replicates are presented as mean ± SD. Some error bars are obscured by plot symbols. (*F*) Quantification of pull-down analyses with purified immobilized His-tagged IraD and purified wild-type RssB and RssB^{AAA}. Shown are means ± SD of three replicates. (****) *P*-value <0.0001, Student's t-test. Sample SDS-PAGE is shown in Supplemental Figure S9D. (*G*) Schematic illustrating the role of RssB plasticity in σ^S turnover. RssB exists in a dynamic equilibrium of multiple conformations, including an "on" state with high affinity for σ^S and "off" states with low affinity for σ^S. Generally, "off" states have mutually inhibitory contacts between the receiver and effector domains, while "on" states generally feature fewer interdomain contacts (Gao and Stock 2010; Corrêa and Gardner 2016). IraD-bound RssB features a "closed" conformation with the interacting NTD and CTD. The interdomain linker containing the glutamate cluster (green) likely functions as a flexing joint to accommodate the binding of multiple inhibitors induced by specific stress signals as well as σ^S and ClpXP and possibly kinases. The use of a highly plastic linker featuring a glutamate cluster is similar to the mechanism for multiple target recognition in the calmodulin system (Supplemental Fig. S12).

phosphorylation to σ-factor regulation. This interplay often relies on modulating the pools of free σ via anti-σ factors, which prevent RNA polymerase holoenzyme formation by sequestration of the σ subunit, and anti-anti-σ factors, which in turn sequester the anti-σ (Gruber and Gross 2003). In both Gram-positives and Gram-negatives, kinases and phosphatases often regulate σ/anti-σ/antianti-σ networks (Gruber and Gross 2003). However,

E. coli and related species use σ^S degradation instead as a major way of partitioning the transcriptional space when mounting a general stress response. This process is dependent on a response regulator (RssB), which plays a catalytic role; i.e., it is not degraded by ClpXP (Fig. 1A). Nonphosphorylatable substitutions at the phosphoacceptor location of RssB, such as D58P and D58A, support σ^S degradation in vivo and in vitro, suggesting that phosphorylation is not the major mode of regulation (Peterson et al. 2004; Battesti et al. 2013). Instead, most regulation is provided by antiadaptors IraD, IraP, and IraM, which titrate RssB to prevent σ^S destruction. These have been proposed to use distinct modes of RssB recognition (Bougdour et al. 2006; Battesti and Gottesman 2013; Battesti et al. 2013; Micevski et al. 2015). Our study elucidates the mechanism of RssB inhibition upon DNA damage by IraD and, importantly, provides a more general mechanistic framework for understanding the functional modulation of response regulators.

First, we demonstrated that IraD binding involves direct interactions with both the RssB NTD and CTD, dependent on a novel compact form of the linker that juxtaposes these domains (Fig. 2). The IraD interaction with both the RssB NTD and CTD was unexpected. Previous work had implicated only the NTD in interactions with IraD (Battesti et al. 2013; Micevski et al. 2015). Indeed, we found that contacts with the RssB NTD are more extensive and critical to function. We identified one residue within the receiver domain, D104, which, when mutated, abolishes IraD binding and significantly reduces function in vitro and in vivo (Fig. 5). On the IraD side, we pinpointed residues R67, R70, and especially W64 as playing key roles in RssB recognition (Fig. 4).

Second, we found that free RssB is a mixture of predominantly monomeric "open" and scarce "closed" forms enabled by the plasticity of its interdomain linker (Fig. 3). We emphasize that the "open" conformation may not be structurally identical to the conformation of the crystallized *P. aeruginosa* homolog, which may not functionally substitute for *E. coli* RssB (Battesti et al. 2013). The *P. aeruginosa* linker sequence is significantly different from that of RssB. First, it does not contain a glutamate cluster or a helix breaker, such as P150 (Supplemental Fig. S1C), arguing against an extended one-helix linker for *E. coli* RssB. In addition, the dimeric *P. aeruginosa* structure features a more rigid coiled–coil stabilized linker (Supplemental Fig. S1A). While RssB oligomerization can be detected by cross-linking (Fig. 3G; Supplemental Fig. S10A), it cannot be detected by SEC-MALS even at concentrations above physiological (Supplemental Fig. S10B) and does not appear to be phosphorylation-dependent, leaving the role of RssB oligomerization unclear.

ClpXP-dependent σ^S degradation consists of several sequential steps: σ^S binding to RssB, transfer of σ^S to ClpXP, unfolding of σ^S by ClpX, translocation of unfolded σ^S to ClpP for proteolysis, and RssB recycling. Regulation can thus be achieved at any of these steps and could involve more than just binding to RssB to prevent its association with σ^S. It could include modulating RssB–σ^S (Battesti et al. 2013) or RssB–σ^S–ClpXP interactions and/or RssB recycling. This is likely the reason behind the difference in sensitivity of some of our in vivo and in vitro assays, which we interpret as being due to competition with σ^S (Battesti et al. 2013) and possibly different extents of phosphorylation. While IraD and IraM interactions with RssB are largely phosphorylation-independent, IraP binding is disfavored by nonphophorylatable (D58P) substitutions and is competitive with σ^S for RssB binding; both σ^S and IraP may share partially overlapping RssB-binding interfaces, including or close to the 4-5-5 face (Battesti et al. 2013). Importantly, in agreement with previous work (Battesti et al. 2013), our data indicate that requirements for antiadaptor binding are not sufficient for antiadaptor sensitivity (Fig. 6). In the case of IraD, the RssB NTD confers enough affinity for IraD for formation of a complex stable enough to be detected by pull-down assays, yet variants carrying mutations beyond the NTD ($RssB^{R115A}$ and particularly $RssB^{Q254A\ N256A}$) bind well but are partially resistant to inhibition in vivo (Fig. 5A,C). R115 is located at the N terminus of α5, which connects directly to the linker helices and likely modulates its conformation and NTD/CTD interactions. Q254 and N256 are located at the C terminus of the switch helix that packs against α5, the site of mutations (class II mutations) (Battesti et al. 2013) that lead to constitutive activation and bypass the need for phosphorylation. This is likely due to disruption of the helical RssB core (Fig. 2C,D), which is conducive to σ^S binding, which would normally be favored by phosphorylation (Battesti et al. 2013). Overall, these earlier findings and our data point to a two-step IraD-binding mode. First, IraD gets recruited via high-affinity contacts with the RssB NTD, which may then trigger closure of the molecule or capture of transient closed forms, leading to formation of fully inhibitory contacts with the RssB CTD. This closed inactive state does not resemble the *P. aeruginosa*-like open structure of RssB, as proposed earlier by Dougan and coworkers (Micevski et al. 2015), and is incompatible with the head-to-head dimerization seen in the *P. aeruginosa* homolog because of IraD docking to the 4-5-5 face.

Last, we show that the RssB polyglutamate motif is crucial for σ^S degradation even in the absence of antiadaptors. While substitution of the polyglutamate motif for a highly flexible GSGS sequence compromises σ^S degradation (Fig. 6) and σ^S binding (Supplemental Fig. S9A), introduction of a more rigid helical AAA sequence has a less severe effect, reducing activity in vivo and in vitro but not affecting σ^S interactions (Fig. 6B–D; Supplemental Fig. S9A). These data argue that the rigidity and reorganization of the linker might be particularly important for fulfilling stringent steric requirements for substrate loading/handoff to ClpXP and RssB recycling. Is the linker then important for regulation by antiadaptors? While $RssB^{AAA}$ appears to be slightly impaired in binding IraD in vitro in the absence of σ^S (Fig. 6F), it remains sensitive in vivo to all antiadaptors (Supplemental Fig. S11). Further structural studies of RssB, particularly in complex with σ^S, will be required to fully answer this question, but a simple explanation for this observation is that $RssB^{AAA}$ can still

interact well enough with IraD through its 4-5-5 face in its intact receiver domain and that this binding event is sufficient to achieve partial inhibition.

To conclude, our study supports earlier proposals that antiadaptors use distinct mechanisms for inhibiting RssB (Battesti et al. 2013; Micevski et al. 2015) and places decades of genetics and biochemical work within a mechanistic framework. None of the previously described mutations that compromise IraD regulation (Battesti et al. 2013) map to the interface with IraD. Two mutations (W143R and P150T) (Fig. 6A) map to the linker sequence; others, the class II mutations, map to an ancestral switch element (Fig. 2A,B) not only present in Ser/Thr phosphatase folds but universally conserved in proteosomal-like proteases (Bradshaw et al. 2017). For activation, these proteases reposition their switch helices upon docking of a regulatory "cap" (Sousa et al. 2000). In SpoIIE, phosphatase activation involves dimerization partially mediated by these switches. In RssB, mutations in this area likely lead to intramolecular rearrangements of the helical core. We highlight the polyglutamate motif within the RssB linker as an important element for σ^s turnover (Fig. 6). Its collapse into shorter α helices and >70 Å displacement of the effector domain (Fig. 2B) are unusual among the response regulators that have been crystallized thus far (Gao and Stock 2010) but are reminiscent of the conformational changes in calmodulin. In free form, calmodulin consists of a dumbbell architecture with a central helical linker connecting Ca^{2+}-binding EF hands (Babu et al. 1985), as shown in Supplemental Fig. S12A. Upon binding to multiple physiological targets, calmodulin undergoes compaction (Meador et al. 1993) via local unfolding of the central helix and its splitting into three shorter helices (Supplemental Fig. S12B,C). Strikingly, like RssB, calmodulin also features a highly conserved glutamate cluster within its helical linker, which has been observed either disordered or in a helical conformation (Supplemental Fig. S12B,C). This study and other work have led to the concept of linker plasticity as underlying the ability of calmodulin to assume conformations capable of recognizing dozens of sequence-dissimilar targets. Charge reversal of this glutamate cluster by mutagenesis differentially affected activation of various calmodulin targets (Craig et al. 1987), demonstrating its functional importance. Like calmodulin, RssB interacts with sequence-dissimilar antiadaptors, kinase, σ^S, and ClpX. Although only three antiadaptors have been identified, the list might be more extensive, reflecting the diversity of environmental stress signals. In fact, σ^S is stabilized by overexpression of transcriptional regulator AppY in strains deleted for *iraD*, *iraM*, and *iraP* (Bougdour et al. 2008), supporting the existence of additional RssB inhibitors. The RssB linker could then serve as an expansion joint that could be adjusted to achieve multiple conformations, possibly allowing for combinatorial and tunable interactions of RssB with kinase, antiadaptors, ClpX, and σ^S (Fig. 6G). Thus, altogether, our work not only reveals the mechanistic underpinnings of IraD-mediated RssB inhibition but extends the remarkable plasticity of response regulator architectures, particularly in complex with modulators, and points to RssB proteins as sharing elements of the calmodulin paradigm.

Materials and methods

Protein expression and purification

E. coli K12 *iraD* and *rssB* genes were amplified by PCR from plasmids pQE80-IraD and pT7-RssB (Battesti et al. 2013), digested, and ligated into pSKB2 (a generous gift from Dr. S. Burley) and pOKD5 (a generous gift from Dr. H. Wu) to generate plasmids pVF14 (His_6IraD), pVF18 (His_6IraD^{Trunc}), pVF16 ($RssB^{D58P}$), and pBD1 (RssB). IraD and RssB mutations were introduced by standard PCR-based site-directed mutagenesis. Plasmids were verified using DNA sequencing. Oligonucleotide sequences used for plasmid construction are listed in Supplemental Table S2. Bacterial plasmids and strains are listed in Supplemental Tables S3 and S4.

For overexpression of IraD•RssB and $IraD^{Trunc}$•$RssB^{D58P}$ complexes, plasmids were transformed into BL21(DE3)-competent cells. Cells were grown in Lennox broth to an OD_{600} of 0.6–0.8 at 37°C in the presence of 25 µg/mL kanamycin and 50 µg/mL carbenicillin. This was followed by induction with 1 mM isopropyl β-D-1-thiogalactopyranoside (IPTG) and further incubation for 4 h at 30°C with shaking. For expression of selenomethionyl-substituted protein, pVF16/pVF18 were cotransformed into Met-auxotroph strain B834(DE3) (EMD Millipore) and grown in SelenoMet medium (Molecular Dimensions).

Hexahistidine-tagged IraD•RssB protein complexes were purified by Ni^{2+}-affinity chromatography followed by cleavage of the affinity tag with PreScission protease and further purification by anion exchange chromatography and SEC on a Superdex 200 Increase 10/300 column (GE Healthcare).

Crystallization, structure determination, and refinement

The $IraD^{Trunc}$•$RssB^{D58P}$ complex was crystallized at room temperature using sitting drop vapor diffusion from a protein solution mixed at a 1:1 ratio with 0.2 M $MgCl_2$, 7.5%–12.5% polyethylene glycol 8000, and 0.1 M Tris (pH 8.5). Crystals were cryoprotected in well solution supplemented with 30% ethylene glycol and flash-cooled in liquid nitrogen.

Data were collected at the Advanced Light Source beamline 5.02. The SAD data set was collected at the peak of the Se K-absorption edge. Both data sets were indexed, reduced, and scaled using HKL2000 (Otwinowski and Minor 1997). Anomalous scatters were located using HySS, and phasing was done using the Phaser-EP module in Phenix (Adams et al. 2002) followed by density modification with RESOLVE (Adams et al. 2002). This procedure yielded electron density maps in which ~75% of the protein chains could be built automatically using Autobuild (Adams et al. 2002). The partial model was refined against the intensities of the higher-resolution data set, also with Phenix (Adams et al. 2002), using a riding hydrogen model. Reflection and refinement statistics are shown in Table 1.

Pull-down assays

For pull-down assays with IraD variants, 67 pmol of purified wild-type or variant His_6IraD was mixed with 160 pmol of purified wild-type RssB at a concentration of 1.6 µM. Proteins were incubated for 20 min on ice in binding buffer (20 mM Tris at pH 8.0, 40 mM imidazole, 250 mM NaCl, 5% glycerol, 2 mM β-mercaptoethanol). The sample was applied to HisPur Ni-NTA resin (Thermo Scientific), equilibrated in binding buffer, and incubated

for 20 min at 4°C with gentle rotation. Beads were washed three times with binding buffer, and then immobilized protein was eluted from the beads with elution buffer (20 mM Tris at pH 8.0, 500 mM imidazole, 250 mM NaCl, 5% glycerol, 2 mM β-mercaptoethanol). Samples were analyzed by SDS-PAGE followed by staining with Coomassie blue. For pull-down assays with RssB variants, His_6IraD was coexpressed with wild-type or variant RssB, and pull-downs were performed on clarified lysates as described above.

For functional studies with purified RssB, we overexpressed wild-type and variant RssB constructs and purified them using nickel-affinity followed by tag cleavage with Prescission protease (where applicable) and SEC on a Superdex 200 10/300 column (GE Healthcare). Pull-down analyses were performed as above except that the concentration of RssB variants applied to beads was increased to 6 µM. Purified RssB constructs were verified using MS.

Interdomain disulfide engineering and cross-linking reactions

For engineering disulfide bonds that would trap RssB in the crystallographically observed closed conformation, we used Disulfide by Design (Dombkowski 2003). This analysis suggested S29 and E229 as good candidates for cysteine substitutions, and these were introduced in our wild-type RssB plasmid. Complexes containing RssB cysteine mutants or wild-type RssB were purified like the $IraD^{Trunc}$•$RssB^{D58P}$ complex used for crystallization.

For cross-linking studies, purified protein was first fully reduced by incubation with 5 mM TCEP for 1 h on ice, and buffer was subsequently exchanged to 0.2 M NaCl and 20 mM Tris (pH 8). Cysteine oxidation by atmospheric oxygen was carried out immediately afterward at a protein concentration of 0.25 mg/mL in the presence of the CuPhen catalyst at concentrations of 0, 5, 10, 15, and 20 µM for 20 min at room temperature; quenched by alkylation with 50 mM iodoacetamide and SDS-loading buffer; and analyzed on 10% SDS-PAGE gels. Cross-linking in Figure 3G was performed with 15 µM CuPhen.

In vitro σ^S degradation assay

ClpX (Grimaud et al. 1998), ClpP (Maurizi et al. 1994), and σ^S (Zhou et al. 2001) were purified as described previously. σ^S was labeled with Alexa fluor 488 carboxylic acid, succinimidyl ester (Thermo Fisher) as recommended by the manufacturer. The degree of labeling was 2 mol/mol. Protein concentrations given are for σ^S, RssB monomers, ClpX hexamers, and ClpP tetradecamers. Degradation reactions (30 µL) were assembled in buffer B (20 mM Tris at pH 7.5, 100 mM KCl, 0.1 mM EDTA, 5 mM DTT, 5% [v/v] glycerol) containing 10 mM $MgCl_2$, 2 mM ATP, 25 mM acetyl phosphate, 0.1 µM ClpX, 0.2 µM ClpP, 2 µM fluorescent σ^S, and RssB as indicated. After incubation for 20 min at 23°C, 70 µL of buffer B containing 15 mM EDTA was added to stop the reactions. Degradation products were isolated with Nanosep 10-kDa MWCO ultrafiltration devices (Pall; prewashed with 20 mM Tris at pH 7.5, 100 mM NaCl, 0.01% Triton X-100) by centrifugation at 14,000*g* for 10 min. Eluent fluorescence was measured using a Tecan M200 Pro plate reader with excitation and emission wavelengths of 490 and 525 nm, respectively. σ^S degradation by ClpXP in the absence of RssB (1.9 pmol ± 0.2 pmol) was subtracted from the data shown. Degradation reactions containing IraD were performed as described above using 0.1 µM wild-type RssB or RssB mutant and IraD as indicated. Data analysis was performed using Prism (Graphpad Software). The degradation end point of 20 min was within the linear phase of degradation as indicated by time-course experiments using the reaction conditions described above.

Monitoring in vivo σ^S degradation

To test the IraD wild-type or mutant activity, strain AB011 (expressing high levels of RssB) or AB007 (expressing physiological levels of RssB) was transformed with pQE80L-IraD, mutant derivatives of pQE80L-IraD, or pQE80L (vector) plasmid (Supplemental Table S2), and transformants were selected at 37°C on LB-agar containing 50 µg/mL ampicillin. A single colony was inoculated into LB containing 100 µg/mL ampicillin and grown overnight at 37°C with shaking. Overnight cultures were diluted 1:500 into fresh LB medium containing 100 µg/mL ampicillin. When cells reached an OD_{600} of 0.3, IraD was induced from the pQE80L IraD plasmid with 100 µM IPTG for 15 min. Global protein synthesis was inhibited by adding 400 µg/mL tetracycline. Where appropriate, 1-mL samples were harvested at various times (0, 10, 20, and 30 min), and TCA precipitation was performed. Samples were resuspended in 75 µL of sample buffer (containing 50 mM Tris-HCl at pH 6.8, 0.2% bromophenol blue, 20% glycerol, 2% SDS) after normalization to cell density.

To test wild-type or variant RssB activity, strains (listed in the figure legends and described in Supplemental Table S4) were transformed with pHDB3 RssB or mutant derivatives containing *rssB* under its native promoter or with the pHDB3 vector plasmid, and transformants were selected at 37°C on LB-agar containing 50 µg/mL ampicillin. A single colony was inoculated into LB containing 100 µg/mL ampicillin and grown overnight at 37°C with shaking. The overnight culture was diluted 1:500 into fresh LB medium containing 100 µg/mL ampicillin and grown to an OD_{600} of 0.3. Global protein synthesis was inhibited by adding 200 µg/mL chloramphenicol. One-milliliter samples were harvested at various times (e.g. 0, 5, 10, and 20 min). For measurement of IraD resistance, strain AT477 (Δ*rssB iraD*^{up}), expressing IraD from a pBAD promoter, was grown to OD 0.2 and induced with 0.2% arabinose for 30 min before adding chloramphenicol. IraP and IraM are expressed from constitutive promoters in strains ST1011 (Δ*rssB iraP*^{UP}) and BA290 (Δ*rssB iraM*^{UP}) and thus were not induced. TCA precipitation was performed, and samples were prepared as described above.

Western blot analysis of σ^S accumulation

Samples were separated by electrophoresis on Nu-PAGE 12% Bis-Tris gel (Invitrogen). Proteins were transferred to nitrocellulose membrane using iBlot Gel transfer block (Life Technologies) and probed with polyclonal rabbit anti-σ^S (1:5000 dilution; Wickner laboratory stock), polyclonal rabbit anti-IraD (1:5000 dilution; Gottesman laboratory stock), and mouse monoclonal anti-EFTU (1:10,000 dilution; LSBio, LS-C128699). Blots were developed with CDP-Star substrate with Nitro-Block-II enhancer (Thermo Scientific) visualized with ChemiDoc (Bio-Rad). Quantification was performed using ImageJ software (National Institutes of Health).

Coordinates and reflection intensities have been deposited in the Protein Data Bank under PDB ID 6OD1.

Acknowledgments

A.M.D. thanks the Berkeley Center for Structural Biology for support, and the Fawzi and Jogl laboratories for generous sharing of equipment. MS was performed at the Keck Proteomics Facility (Yale University) by N. Rauniyar and J. Kanyo. SEC-MALS was performed by Dr. A. Grigorescu (Keck Biophysical Facility at Northwestern University). This research is based in part on work conducted using the Rhode Island National Science Foundation/Established Program to Stimulate Competitive Research

(EPSCoR) Proteomics and Structural Biology Facilities at Brown University. Work in the laboratory of A.M.D. was funded by R01GM121975 from the National Institutes of Health (NIH) and a Salomon Research Award from Brown University. Work in the laboratories of S.G. and S.W. is supported by the Intramural Research Program of the NIH, National Cancer Institute, Center for Cancer Research.

Author contribution: V.D. performed cloning for protein purification, protein purification, crystallization, and cross-linking. C.B., M.M.S., and A.S. prepared reagents for and carried out circular dichroism, chemical cross-linking, pull-down, and limited proteolysis assays. A.T. and S.T. performed cloning for and carried out in vivo analyses of interactions and activities. J.R.H. carried out in vitro studies on σ^S degradation. A.M.D., S.G., and S.W. designed and discussed experimental approaches and interpretation. A.M.D. directed the project; flash-cooled crystals; collected X-ray data; solved, refined, and analyzed the crystal structure; and wrote the manuscript with input from all of the authors.

References

Adams JL, McLean RJ. 1999. Impact of rpoS deletion on *Escherichia coli* biofilms. *Appl Environ Microbiol* **65:** 4285–4287.

Adams PD, Grosse-Kunstleve RW, Hung LW, Ioerger TR, McCoy AJ, Moriarty NW, Read RJ, Sacchettini JC, Sauter NK, Terwilliger TC. 2002. PHENIX: building new software for automated crystallographic structure determination. *Acta Crystallogr D Biol Crystallogr* **58:** 1948–1954. doi:10.1107/S0907444902016657

Babu YS, Sack JS, Greenhough TJ, Bugg CE, Means AR, Cook WJ. 1985. Three-dimensional structure of calmodulin. *Nature* **315:** 37–40. doi:10.1038/315037a0

Basler M, Pilhofer M, Henderson GP, Jensen GJ, Mekalanos JJ. 2012. Type VI secretion requires a dynamic contractile phage tail-like structure. *Nature* **483:** 182–186. doi:10.1038/nature10846

Battesti A, Gottesman S. 2013. Roles of adaptor proteins in regulation of bacterial proteolysis. *Curr Opin Microbiol* **16:** 140–147. doi:10.1016/j.mib.2013.01.002

Battesti A, Majdalani N, Gottesman S. 2011. The RpoS-mediated general stress response in *Escherichia coli*. *Annu Rev Microbiol* **65:** 189–213. doi:10.1146/annurev-micro-090110-102946

Battesti A, Hoskins JR, Tong S, Milanesio P, Mann JM, Kravats A, Tsegaye YM, Bougdour A, Wickner S, Gottesman S. 2013. Anti-adaptors provide multiple modes for regulation of the RssB adaptor protein. *Genes Dev* **27:** 2722–2735. doi:10.1101/gad.229617.113

Bearson SM, Benjamin WH Jr, Swords WE, Foster JW. 1996. Acid shock induction of RpoS is mediated by the mouse virulence gene MviA of *Salmonella typhimurium*. *J Bacteriol* **178:** 2572–2579. doi:10.1128/jb.178.9.2572-2579.1996

Becker G, Klauck E, Hengge-Aronis R. 1999. Regulation of RpoS proteolysis in *Escherichia coli*: the response regulator RssB is a recognition factor that interacts with the turnover element in RpoS. *Proc Natl Acad Sci* **96:** 6439–6444. doi:10.1073/pnas.96.11.6439

Bouché S, Klauck E, Fischer D, Lucassen M, Jung K, Hengge-Aronis R. 1998. Regulation of RssB-dependent proteolysis in *Escherichia coli*: a role for acetyl phosphate in a response regulator-controlled process. *Mol Microbiol* **27:** 787–795. doi:10.1046/j.1365-2958.1998.00725.x

Bougdour A, Wickner S, Gottesman S. 2006. Modulating RssB activity: IraP, a novel regulator of σ^S stability in *Escherichia coli*. *Genes Dev* **20:** 884–897. doi:10.1101/gad.1400306

Bougdour A, Cunning C, Baptiste PJ, Elliott T, Gottesman S. 2008. Multiple pathways for regulation of σ^S (RpoS) stability in *Escherichia coli* via the action of multiple anti-adaptors. *Mol Microbiol* **68:** 298–313. doi:10.1111/j.1365-2958.2008.06146.x

Bradshaw N, Levdikov VM, Zimanyi CM, Gaudet R, Wilkinson AJ, Losick R. 2017. A widespread family of serine/threonine protein phosphatases shares a common regulatory switch with proteasomal proteases. *eLife* **6:** e26111. doi:10.7554/eLife.26111

Casino P, Rubio V, Marina A. 2009. Structural insight into partner specificity and phosphoryl transfer in two-component signal transduction. *Cell* **139:** 325–336. doi:10.1016/j.cell.2009.08.032

Chen X, Zaro JL, Shen WC. 2013. Fusion protein linkers: property, design and functionality. *Adv Drug Deliv Rev* **65:** 1357–1369. doi:10.1016/j.addr.2012.09.039

Corrêa F, Gardner KH. 2016. Basis of mutual domain inhibition in a bacterial response regulator. *Cell Chem Biol* **23:** 945–954. doi:10.1016/j.chembiol.2016.07.010

Craig TA, Watterson DM, Prendergast FG, Haiech J, Roberts DM. 1987. Site-specific mutagenesis of the α-helices of calmodulin. Effects of altering a charge cluster in the helix that links the two halves of calmodulin. *J Biol Chem* **262:** 3278–3284.

Daggett V, Kollman PA, Kuntz ID. 1991. A molecular dynamics simulation of polyalanine: an analysis of equilibrium motions and helix-coil transitions. *Biopolymers* **31:** 1115–1134. doi:10.1002/bip.360310911

Dombkowski AA. 2003. Disulfide by design: a computational method for the rational design of disulfide bonds in proteins. *Bioinformatics* **19:** 1852–1853. doi:10.1093/bioinformatics/btg231

Dong T, Schellhorn HE. 2009. Global effect of RpoS on gene expression in pathogenic *Escherichia coli* O157:H7 strain Edl933. *BMC Genomics* **10:** 349. doi:10.1186/1471-2164-10-349

Dong T, Schellhorn HE. 2010. Role of RpoS in virulence of pathogens. *Infect Immun* **78:** 887–897. doi:10.1128/IAI.00882-09

Dong T, Kirchhof MG, Schellhorn HE. 2008. RpoS regulation of gene expression during exponential growth of *Escherichia coli* K12. *Mol Genet Genomics* **279:** 267–277. doi:10.1007/s00438-007-0311-4

Galperin MY. 2006. Structural classification of bacterial response regulators: diversity of output domains and domain combinations. *J Bacteriol* **188:** 4169–4182. doi:10.1128/JB.01887-05

Gao R, Stock AM. 2010. Molecular strategies for phosphorylation-mediated regulation of response regulator activity. *Curr Opin Microbiol* **13:** 160–167. doi:10.1016/j.mib.2009.12.009

Grimaud R, Kessel M, Beuron F, Steven AC, Maurizi MR. 1998. Enzymatic and structural similarities between the *Escherichia coli* ATP-dependent proteases, ClpXP and ClpAP. *J Biol Chem* **273:** 12476–12481. doi:10.1074/jbc.273.20.12476

Gruber TM, Gross CA. 2003. Multiple σ subunits and the partitioning of bacterial transcription space. *Annu Rev Microbiol* **57:** 441–466. doi:10.1146/annurev.micro.57.030502.090913

Hengge-Aronis R. 2002. Signal transduction and regulatory mechanisms involved in control of the σ^S (RpoS) subunit of RNA polymerase. *Microbiol Mol Biol Rev* **66:** 373–395. doi:10.1128/MMBR.66.3.373-395.2002

Herrou J, Rotskoff G, Luo Y, Roux B, Crosson S. 2012. Structural basis of a protein partner switch that regulates the general stress response of α-proteobacteria. *Proc Natl Acad Sci* **109:** E1415–E1423. doi:10.1073/pnas.1116887109

Ito A, May T, Kawata K, Okabe S. 2008. Significance of RpoS during maturation of *Escherichia coli* biofilms. *Biotechnol Bioeng* **99:** 1462–1471. doi:10.1002/bit.21695

Ito A, May T, Taniuchi A, Kawata K, Okabe S. 2009. Localized expression profiles of RpoS in *Escherichia coli* biofilms. *Biotechnol Bioeng* **103:** 975–983. doi:10.1002/bit.22305

Janin J, Miller S, Chothia C. 1988. Surface, subunit interfaces, and interior of oligomeric proteins. *J Mol Biol* **204:** 155–164. doi:10.1016/0022-2836(88)90606-7

Joshi KK, Bergé M, Radhakrishnan SK, Viollier PH, Chien P. 2015. An adaptor hierarchy regulates proteolysis during a bacterial cell cycle. *Cell* **163:** 419–431. doi:10.1016/j.cell.2015.09.030

Kelley LA, Mezulis S, Yates CM, Wass MN, Sternberg MJ. 2015. The Phyre2 web portal for protein modeling, prediction and analysis. *Nat Protoc* **10:** 845–858. doi:10.1038/nprot.2015.053

Krejtschi C, Hauser K. 2011. Stability and folding dynamics of polyglutamic acid. *Eur Biophys J* **40:** 673–685. doi:10.1007/s00249-011-0673-8

Lacour S, Landini P. 2004. σ^S-dependent gene expression at the onset of stationary phase in *Escherichia coli:* function of σ^S-dependent genes and identification of their promoter sequences. *J Bacteriol* **186:** 7186–7195. doi:10.1128/JB.186.21.7186-7195.2004

Lange R, Hengge-Aronis R. 1991a. Growth phase-regulated expression of bolA and morphology of stationary-phase *Escherichia coli* cells are controlled by the novel σ factor σ^S. *J Bacteriol* **173:** 4474–4481. doi:10.1128/jb.173.14.4474-4481.1991

Lange R, Hengge-Aronis R. 1991b. Identification of a central regulator of stationary-phase gene expression in *Escherichia coli*. *Mol Microbiol* **5:** 49–59. doi:10.1111/j.1365-2958.1991.tb01825.x

Lossi NS, Dajani R, Freemont P, Filloux A. 2011. Structure–function analysis of HsiF, a Gp25-like component of the type VI secretion system, in *Pseudomonas aeruginosa*. *Microbiology* **157:** 3292–3305. doi:10.1099/mic.0.051987-0

Maeda H, Fujita N, Ishihama A. 2000. Competition among seven *Escherichia coli* σ subunits: relative binding affinities to the core RNA polymerase. *Nucleic Acids Res* **28:** 3497–3503. doi:10.1093/nar/28.18.3497

Mahmoud SA, Chien P. 2018. Regulated proteolysis in bacteria. *Annu Rev Biochem* **87:** 677–696. doi:10.1146/annurev-biochem-062917-012848

Maurizi MR, Thompson MW, Singh SK, Kim SH. 1994. Endopeptidase Clp: ATP-dependent Clp protease from *Escherichia coli*. *Methods Enzymol* **244:** 314–331. doi:10.1016/0076-6879(94)44025-5

Meador WE, Means AR, Quiocho FA. 1993. Modulation of calmodulin plasticity in molecular recognition on the basis of X-ray structures. *Science* **262:** 1718–1721. doi:10.1126/science.8259515

Merrikh H, Ferrazzoli AE, Lovett ST. 2009. Growth phase and (p)ppGpp control of IraD, a regulator of RpoS stability, in *Escherichia coli*. *J Bacteriol* **191:** 7436–7446. doi:10.1128/JB.00412-09

Micevski D, Zammit JE, Truscott KN, Dougan DA. 2015. Anti-adaptors use distinct modes of binding to inhibit the RssB-dependent turnover of RpoS (σ^S) by ClpXP. *Front Mol Biosci* **2:** 15. doi:10.3389/fmolb.2015.00015

Mika F, Hengge R. 2005. A two-component phosphotransfer network involving ArcB, ArcA, and RssB coordinates synthesis and proteolysis of σ^S (RpoS) in *E. coli*. *Genes Dev* **19:** 2770–2781. doi:10.1101/gad.353705

Mitrophanov AY, Groisman EA. 2008. Signal integration in bacterial two-component regulatory systems. *Genes Dev* **22:** 2601–2611. doi:10.1101/gad.1700308

Muffler A, Fischer D, Altuvia S, Storz G, Hengge-Aronis R. 1996. The response regulator RssB controls stability of the σ^S subunit of RNA polymerase in *Escherichia coli*. *EMBO J* **15:** 1333–1339. doi:10.1002/j.1460-2075.1996.tb00475.x

Otwinowski Z, Minor W. 1997. Processing of X-ray diffraction data collected in oscillation mode. *Methods Enzymol* **276:** 307–326. doi:10.1016/S0076-6879(97)76066-X

Patten CL, Kirchhof MG, Schertzberg MR, Morton RA, Schellhorn HE. 2004. Microarray analysis of RpoS-mediated gene expression in *Escherichia coli* K-12. *Mol Genet Genomics* **272:** 580–591. doi:10.1007/s00438-004-1089-2

Peano C, Wolf J, Demol J, Rossi E, Petiti L, De Bellis G, Geiselmann J, Egli T, Lacour S, Landini P. 2015. Characterization of the *Escherichia coli* σ^S core regulon by chromatin immunoprecipitation-sequencing (ChIP-seq) analysis. *Sci Rep* **5:** 10469. doi:10.1038/srep10469

Peterson CN, Ruiz N, Silhavy TJ. 2004. RpoS proteolysis is regulated by a mechanism that does not require the SprE (RssB) response regulator phosphorylation site. *J Bacteriol* **186:** 7403–7410. doi:10.1128/JB.186.21.7403-7410.2004

Pratt LA, Silhavy TJ. 1996. The response regulator SprE controls the stability of RpoS. *Proc Natl Acad Sci* **93:** 2488–2492. doi:10.1073/pnas.93.6.2488

Pruteanu M, Hengge-Aronis R. 2002. The cellular level of the recognition factor RssB is rate-limiting for σ^S proteolysis: implications for RssB regulation and signal transduction in σ^S turnover in *Escherichia coli*. *Mol Microbiol* **45:** 1701–1713. doi:10.1046/j.1365-2958.2002.03123.x

Schweder T, Lee KH, Lomovskaya O, Matin A. 1996. Regulation of *Escherichia coli* starvation σ factor (σ^S) by ClpXP protease. *J Bacteriol* **178:** 470–476. doi:10.1128/jb.178.2.470-476.1996

Sousa MC, Trame CB, Tsuruta H, Wilbanks SM, Reddy VS, McKay DB. 2000. Crystal and solution structures of an HslUV protease-chaperone complex. *Cell* **103:** 633–643. doi:10.1016/S0092-8674(00)00166-5

Studemann A, Noirclerc-Savoye M, Klauck E, Becker G, Schneider D, Hengge R. 2003. Sequential recognition of two distinct sites in σ^S by the proteolytic targeting factor RssB and ClpX. *EMBO J* **22:** 4111–4120. doi:10.1093/emboj/cdg411

Trajtenberg F, Imelio JA, Machado MR, Larrieux N, Marti MA, Obal G, Mechaly AE, Buschiazzo A. 2016. Regulation of signaling directionality revealed by 3D snapshots of a kinase:regulator complex in action. *eLife* **5:** e21422. doi:10.7554/eLife.21422

Trivedi MV, Laurence JS, Siahaan TJ. 2009. The role of thiols and disulfides on protein stability. *Curr Protein Pept Sci* **10:** 614–625. doi:10.2174/138920309789630534

Weber H, Polen T, Heuveling J, Wendisch VF, Hengge R. 2005. Genome-wide analysis of the general stress response network in *Esαherichia coli*: σ^S-dependent genes, promoters, and σ factor selectivity. *J Bacteriol* **187:** 1591–1603. doi:10.1128/JB.187.5.1591-1603.2005

Wong GT, Bonocora RP, Schep AN, Beeler SM, Lee Fong AJ, Shull LM, Batachari LE, Dillon M, Evans C, Becker CJ, et al. 2017. The genome-wide transcriptional response to varying RpoS levels in *Escherichia coli* K-12. *J Bacteriol* **199:** e00755-16. doi:10.1128/JB.00755-16

Zhou Y, Gottesman S. 1998. Regulation of proteolysis of the stationary-phase σ factor RpoS. *J Bacteriol* **180:** 1154–1158.

Zhou Y, Gottesman S, Hoskins JR, Maurizi MR, Wickner S. 2001. The RssB response regulator directly targets σ^S for degradation by ClpXP. *Genes Dev* **15:** 627–637. doi:10.1101/gad.864401